 CMES, vol.16, no.1, pp.41-55, 2006

Multiscale Simulation of Nanoindentation Using the Generalized Interpolation Material Point (GIMP) Method, Dislocation Dynamics (DD) and Molecular Dynamics (MD)

Jin Ma, Yang Liu, Hongbing Lu, and Ranga Komanduri[1]

Abstract: A multiscale simulation technique coupling three scales, namely, the molecular dynamics (MD) at the atomistic scale, the discrete dislocations at the meso scale and the generalized interpolation material point (GIMP) method at the continuum scale is presented. Discrete dislocations are first coupled with GIMP using the principle of superposition (van der Giessen and Needleman (1995)). A detection band seeded in the MD region is used to pass the dislocations to and from the MD simulations (Shilkrot, Miller and Curtin (2004)). A common domain decomposition scheme for each of the three scales was implemented for parallel processing. Simulations of indentation were performed on the (111) plane of Cu at 0 ° K using a cylindrical indenter. The effects of indenter radius and indentation speed on the indentation load-depth curve and nucleation of dislocations were investigated. For simulations at finite temperatures, spatially averaged velocities were used to reduce atom vibrations in the transition region to achieve seamless coupling. Simulations were also performed at different temperatures using a wedge indenter.

keyword: Multiscale Simulation, GIMP, MD, Discrete Dislocations, Nanoindentation, Coupling, Mesoplasticity

1 Introduction

Multiscale modeling has been receiving increasing attention in modeling material behavior in recent time due to its unique capability to simulate and link physical events occurring at various spatial and temporal scales. At the atomic scale, simulation techniques based on atom motion, such as molecular dynamics (MD) and Monte Carlo (MC) simulations can reveal the fundamental aspects of material deformation provided the amount of computation is accommodated by the current computing power and appropriate interatomic potentials used (Raff, Malshe, Hagan, Doughan, Rockley, and Komanduri (2005)). At larger scales, where atomistic simulation cannot be readily applied due to excessive computing cost, techniques such as discrete dislocation dynamics and crystal plasticity (Liu, Wang, Yoshino, Roy, Lu and Komanduri (2005); Hasebe (2006)) at the mesoscopic level and finite element analysis at the macroscopic level have been employed. With appropriate coupling techniques, simulation at different scales can be bridged to obtain accurate information in areas where atomistic resolution is desired while allowing the dislocation and continuum descriptions to model the material behaviors in areas farther away without significant loss of accuracy.

Several techniques have been proposed for simulations bridging two or more scales (Kohlhoff, Gumbsch and Fischmeister (1991); Shilkrot, Miller and Curtin (2004); Curtin and Miller (2003); Shiari, Miller and Curtin (2005); Raffi-Tabar, Hua and Cross (1998); Tewary and Read (2004); Shen and Atluri (2004 a, b, c); Shen and Atluri (2005)). At each individual scale, simulation techniques have been well established. However, the treatment at the transition region, or the handshake region, overlapped by the outer boundary of the atomistic region and the inner boundary of the continuum region is where the difficulties arise (Kohlhoff, Gumbsch and Fischmeister (1991); Shilkrot, Miller and Curtin (2004); Curtin and Miller (2003); Shen and Atluri (2004a)). For example, in multiscale simulation, the finite element method (FEM) is often used at the continuum level. However, spurious effects can occur when waves with the wavelength larger than the element size are transmitted from the MD region into the continuum region, and waves with wavelength smaller than the element size are reflected back artificially (Raffi-Tabbar, Hua and Cross (1998)), causing artificial overheating in the MD region. Efforts were made to minimize the wave reflection while enforcing the displacement and force continuity, as well as energy conser-

[1] Correspondence author, Email: ranga@ceat.okstate.edu. School of Mechanical and Aerospace Engineering, Oklahoma State University, Stillwater, OK 74078.

vation in the handshake region. Cai, de Koning, Bulatov and Yip (2000) proposed the Green's function method in dynamic coupling between the two regions and this technique shows advantages in minimizing the wave reflection. Shen and Atluri (2004c) decomposed the atom displacements into long and short wave-length components in the equivalent continuum region to achieve seamless multiscale simulation. Shen and Atluri (2005) further developed a tangent stiffness formulation for coupling between the meshless local Petrov-Galerkin (MLPG) and MD, where the displacements of the nodes and atoms are solved in one coupled set of linear equations so that the internal forces are balanced at the transition region. Another multi-scale framework merging two scales, the microscale and the continuum scale, was developed to create a hybrid elasto-viscoplastic simulation model coupling discrete dislocation dynamics with finite element analysis based on the principle of superposition (Zbib and Diaz de la Rubia (2002)). At intermediate scale, the dislocation modeling was used in bridging the continuum and atomistic simulations (Raffi-Tabar, Hua and Cross (1998)). The involvement of dislocation dynamics in connecting the atomistic and continuum scales enables the model to handle plastic deformation through the explicit motion of dislocation defects in the continuum region. With this feature, the multiscale model is completely structured for applications, such as nanoindentation (Shiari, Miller and Curtin (2005)).

Plastic deformation in crystalline metals is the result of motion of large number of dislocations. Various discrete dislocation (DD) models have been developed in the past two decades, and dislocations are usually described as line singularities in an elastic medium (Amodeo and Ghoniem (1990); Gulluoglu and Hartley (1992); Kubin and Canova (1992); Fang and Dahl (1993); Groma and Pawley (1993); van der Giessen and Needleman (1995); Zbib, Rhee and Hirth (1998)). On the interactions of the dislocations, the long-range forces are well-represented by the linear elastic fields outside a dislocation core radius of about five Burgers vectors from a dislocation. Within a distance of several Burgers vectors from the core, the displacement field around the dislocation is nonlinear and cannot be described accurately by linear elasticity (Amodeo and Ghoniem (1990)). Instead, a set of constitutive rules were used to represent the short range interactions between dislocations. Recently, nonlinear deformation has been considered in coupling to represent the physical phenomenon. The coupled atomistic/continuum discrete dislocation (CADD) method has demonstrated its capability in detecting dislocations in the atomistic region and converting the atomistic dislocations into discrete dislocations in the continuum region (Shilkrot, Miller and Curtin (2004)). A dynamic version of the CADD method has been used to study the nanoindentation process as a function of temperature and velocity of indentation (Shiari, Miller and Curtin (2005)).

While FEM has been developed as an appealing simulation technique at the continuum scale, it is subjected to some difficulties, including the complexity in mesh generation for computational bodies with complex geometries and severe mesh distortion under large nonlinear deformations. To overcome some of the limitations of FEM, the material point method (MPM) (Sulsky, Zhou and Schreyer (1995); Sulsky and Schreyer (1996)) was introduced for dynamic simulations and the general interpolation material point (GIMP) method (Bardenhagen and Kober (2004)) was presented with improved simulation stability. In these methods, material points that can conform to the geometry complexity with ease are used to discretize the computational body. Further, these methods can avoid the mesh entanglement problem because of the use of Lagrangian description for material points carrying physical quantities and the use of Eulerian description for convection of physical variables and solution of field equations. Wang, Karuppiah, Lu, Roy, and Komanduri (2005) developed an algorithm to use irregular grid in MPM for adaptive mesh. Ma, Lu, and Komanduri (2006) introduced the structured mesh refinement technique in GIMP to model structures with stress concentration effectively. Lu, Daphalapurkar, Wang, Roy and Komanduri (2006) developed a method to seamlessly couple MD and MPM based on one-to-one corresondence of the atoms and the material points in the transition region. To overcome the stability problem of MPM (Bardenhagen and Kober (2004)), a method for multiscale simulation bridging two scales, namely, the continuum scale using the GIMP method and the atomistic scale using MD was proposed and verified in 2D using the multilevel refinement technique in a parallel computing environment (Ma, Lu, Wang, Roy, Hornung, Wissink and Komanduri (2005); Ma, Lu, Wang, Hornung, Wissink and Komanduri (2006)). Coupling between GIMP and MD is achieved by using compatible deformation, force, and energy fields in the transition re-

gion between GIMP and MD. This coupling framework can overcome some inherent limitations of FEM, while maintaining the advantages of the multiscale modeling with a scheme for time-saving in parallel computing.

In this paper, we present a multiscale simulation scheme, encompassing GIMP at the continuum scale, MD at the atomistic scale, and DD at the mesoscale to link GIMP and MD. The technique has expanded the previous GIMP and MD coupling method (Ma, Lu, Wang, Hornung, Wissink and Komanduri (2006)) by introducing discrete dislocations in the framework of coupling. Dislocation accommodation and propagation mechanisms are introduced by detecting dislocations through the MD simulation in real time and then passing them through the boundary. This facilitates in alleviating the artificial wave propagation problem in direct GIMP and MD coupling. The new method can handle larger numerical model without drastically increasing the computational costs, as the introduction of DD allows some regions previously modeled by MD to be simulated by DD. DD can substitute MD in simulating some of the critical areas without significant loss of accuracy and the computation is more economical for the same model.

2 Coupling scheme among GIMP, DD, and MD

2.1 Coupling of GIMP and MD

In this section, we briefly review an algorithm that couples the continuum scale with the atomistic scale directly. At the continuum scale, the generalized interpolation material point (GIMP) method is used. Fig. 1 illustrates the coupling scheme in which the atomistic region is embedded in the continuum region, as shown in Fig. 1 (a). A transition region, where the communication between the two regions takes place, is constructed by overlapping the material points and the atoms by certain width and is divided into three zones, namely, the inner zone, the "incommunicado" zone, and the outer zone, as shown in Fig. 1 (b). A common background grid is used to carry out the communication by interpolating the physical quantities, such as the velocity and forces, back and forth between the continuum region and the atomistic region. The material points in the inner zone, shown in Fig. 1 (b), are updated from atomistic simulation, and then join the rest of the material points in the GIMP simulation. The velocities of the atoms in the outer zone are updated by the continuum region, and then boundary conditions are provided for the MD simulation.

Refinement algorithms in GIMP have been developed to split the material points to the size of atoms at the transition region to achieve seamless coupling. However, if dislocations cannot be modeled explicitly in the continuum region, the atomistic region has to be large enough so that the dislocations do not propagate to the transition region to allow the continuum region to remain elastic.

2.2 Bridging the continuum and atomistic scales with DD

In order to detect dislocations when they are generated in the MD region and then pass them into the continuum region, the method for dislocation detection and passing proposed by Shilkrot, Miller and Curtin (2004) was implemented into the GIMP and MD coupling. Several layers of atoms at the border of the MD region and the continuum region form the detection band elements which are triangular in shape. During deformation, the Lagrangian strain tensor, $\mathbf{E}$, of an element in the detection band is given by (Shilkrot, Miller and Curtin (2004))

$$\mathbf{E} = \frac{1}{2}[\mathbf{F}^T\mathbf{F} - \mathbf{I}] \tag{1}$$

where $\mathbf{I}$ is the second order identity tensor, $\mathbf{F}$ is the deformation gradient tensor and it is decomposed into

$$\mathbf{F} = \mathbf{F}^e\mathbf{F}^p. \tag{2}$$

In Eq. (2), $\mathbf{F}^e$ is related to the lattice stretching while $\mathbf{F}^p$corresponds to the plastic shearing of the slip systems of the crystal. For the case of ideal slip deformation, $\mathbf{F}^e = \mathbf{I}$. $\mathbf{F}^p$can be represented by

$$\mathbf{F}^p = \mathbf{R}\left(\mathbf{I} + \frac{\mathbf{b}\otimes\mathbf{m}}{d}\right), \tag{3}$$

where $\mathbf{R}$ is the lattice rotation and d is the interplanar distance, $\mathbf{b}$ and $\mathbf{m}$ are the Burgers vector and the normal vector of the slip plane, respectively. Substituting Eq. (3) into Eq.(1) , we get the plastic slip strain tensor as

$$\mathbf{E}^p = \frac{1}{2}[(\mathbf{F}^p)^T\mathbf{F}^p - \mathbf{I}] = \frac{(\mathbf{b}\otimes\mathbf{m})_{sym}}{d} + \frac{(\mathbf{m}\otimes\mathbf{b})(\mathbf{b}\otimes\mathbf{m})}{2d^2} \tag{4}$$

For each of the detection band elements, both the actual strain $\mathbf{E}$ and the plastic slip strain $\mathbf{E}^p$ are computed after the positions of the atoms are updated at each computational step. The norm L_2 represents the difference

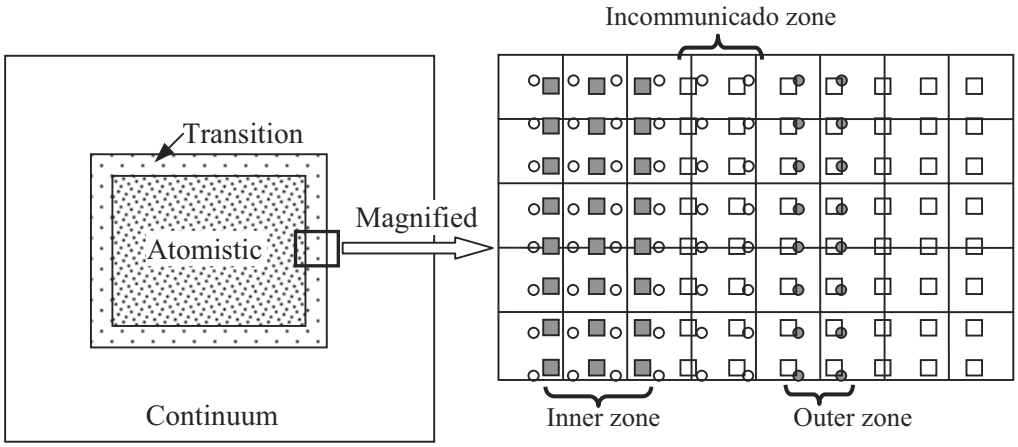

(a) Overall regions of a model (b) Transition region with background grid

Figure 1 : Illustration of coupled GIMP and MD simulations. The circles represent atoms and squares (smaller than physical size) material points. The material points connect to each other without a gap to represent the continuum

between the actual strain and the plastic slip strain.

$$L_2 = \sqrt{(\mathbf{E}-\mathbf{E}_i^p) : (\mathbf{E}-\mathbf{E}_i^p)} \tag{5}$$

If the zero Burgers vector ($\mathbf{b}=\mathbf{0}$) minimizes L_2, no dislocations are detected. Otherwise, the core of the detected dislocation is assigned to the centroid of the detection band element. For 2D triangular lattices, $\mathbf{E}$ can be computed from constant strain triangles as in finite element method (FEM).

Once the dislocations reside in the continuum region, the field variables of the body with the instantaneous dislocation distribution can be solved by the discrete dislocation technique (Kubin and Canova (1992); van der Giessen and Needleman (1995)). Each dislocation i is characterized by its Burgers vector $\mathbf{b}^i$ and the unit normal vector $\mathbf{m}^i$ of its slip plane. The current state of the body in terms of the displacement, strain, and stress fields is computed as the superposition of two fields,

$$\mathbf{u} = \tilde{\mathbf{u}} + \hat{\mathbf{u}}, \quad \varepsilon = \tilde{\varepsilon} + \hat{\varepsilon}, \quad \sigma = \tilde{\sigma} + \hat{\sigma} \tag{6}$$

where the ($\sim$) fields are the fields associated with N dislocations in their current configuration but in an infinite homogeneous medium. The complimentary ($\wedge$) fields are used to enforce the correct boundary conditions. The solution for $\tilde{\sigma}$, $\tilde{\varepsilon}$, and $\tilde{\mathbf{u}}$ is the superposition of the fields of individual dislocations:

$$\tilde{\sigma} = \sum_{i=1}^{N} \tilde{\sigma}^i, \quad \tilde{\varepsilon} = \sum_{i=1}^{N} \tilde{\varepsilon}^i, \quad \tilde{\mathbf{u}} = \sum_{i=1}^{N} \tilde{\mathbf{u}}^i \tag{7}$$

where the analytical solutions $\tilde{\sigma}^i$, $\tilde{\varepsilon}^i$, and $\tilde{\mathbf{u}}^i$ of the individual field are available for straight dislocations in 2D stress state in an infinitely large isotropic material (Hirth and Lothe (1982)).

On the update of dislocations, the Peach-Koehler (P-K) force p^i is the driving force for the evolution in the dislocation topology and it is computed by

$$p^i = (\mathbf{m}^i)^T \cdot (\hat{\sigma} + \sum_{j \neq i}^{N} \tilde{\sigma}^j) \cdot \mathbf{b}^i. \tag{8}$$

Using the linear drag relation, the magnitude of the glide velocity of dislocation i, v^i is computed from the Peach-Koehler force through

$$p^i = Bv^i, \tag{9}$$

where B is the drag coefficient. Then each dislocation i is displaced by $v^i \Delta t$, followed by the determination of the stress and strain state for the updated dislocation structure.

2.3 Parallel processing

The parallel processing scheme for coupling GIMP with MD has been developed using domain decomposition for both MD and GIMP (Ma, Lu, Wang, Hornung, Wissink and Komanduri (2006)). It is noted that only the finest level of GIMP is coupled with MD. The MD code used in this paper is the LAMMPS code (Plimpton (1995)) developed at the Sandia National Laboratories. For all

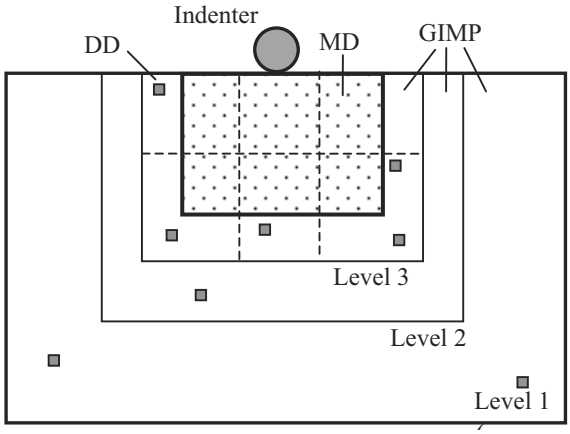

Figure 2 : Illustration of the domain decomposition and refinement for the coupling simulation of 2D indentation using GIMP, DD and MD

the coarser levels, pure GIMP calculation is carried out. When the discrete dislocation is incorporated into the coupling algorithm, care must be taken in the multi processor distributed processing. The DD algorithm shows that the amount of computation related to DD is proportional to N^2, where N is the number of dislocations.

In this investigation, the computational cost of DD is much less than that of MD and GIMP. Hence, we still adopt the same physical domain decomposition as in GIMP for DD. Fig. 2 is a schematic of an indentation problem used in the coupling simulation. The area immediately beneath the indenter is modeled by MD. Three levels of successive refinements in GIMP are shown with the finest level decomposed into six rectangular patches. Other levels are also divided into six patches and these patches are not shown. To reduce data transferring among processors in coupling, the MD region is decomposed into six rectangular regions. Each MD region in coupling is assigned to a patch residing in the same processor as used for the simulation of a GIMP region. Thus, each processor handles both MD and GIMP regions in coupling. Although using the same domain decomposition for MD and GIMP in the finest level does not produce the best load balance among the processors, this approach is simple to implement and effective in the communication between GIMP and MD in the transition region. This is because material points and atoms in exchange of information are stored and processed by the same processor. Hence, no inter-processor communication is necessary.

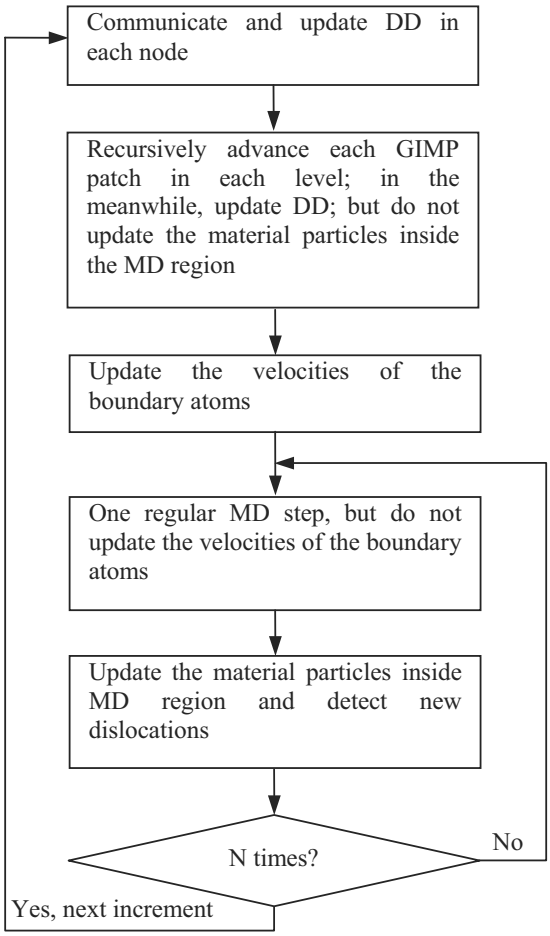

Figure 3 : Flow chart of the coupling algorithm for each increment

When discrete dislocations, shown as small squares in Fig. 2, are introduced into the model, we keep the domain decomposition intact. Fig. 3 shows the overall flowchart of the coupling algorithm incorporating GIMP, DD and MD. Each DD is updated within each patch where it resides because the local continuum stress is needed to compute the Peach-Koehler force applied on it. Because the long-range forces from all other DDs have to be computed, i.e., loop all the DDs, we store the updated information of all the DDs' in each processor. Hence, inter-processor communication can be avoided. The cost is that after each step, i.e., after all patches in each level and the DDs are updated, the updated DD information has to be transmitted to other processors. To achieve this, firstly, each processor sends the local updated DD information, including newly created DDs, to one master node and the master node assembles all the

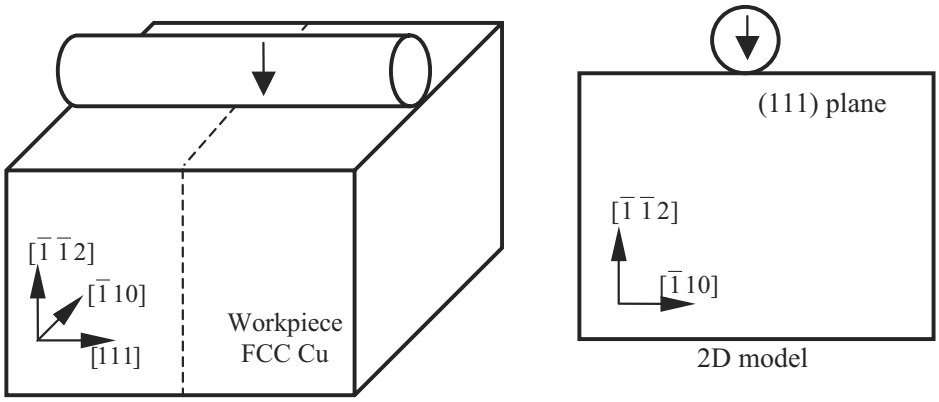

Figure 4 : 2D modeling of an indentation problem with a cylindrical indenter

updated dislocations. Next, the master node broadcasts all the dislocation information to all other processors. It may be noted that each dislocation carries a position and a Burgers vector (four double variables in 2D) and the communication overhead is usually negligible compared to GIMP and MD computations.

2.4 Contact solver for MD

The contact algorithm to determine the contact force for each atom that penetrates into the rigid indenter is more straightforward at the atomistic scale than at the continuum scale. A repulsive potential between the indenter and the atoms in contact can be defined as a function of the penetration depth in the form

$$\Phi = K \cdot ||\mathbf{d}||^n \tag{10}$$

where **d** is the shortest penetration depth vector measured from the atom to the indenter surface, K is a constant that controls the strength of the repulsive potential. The exponent n was chosen as 3 in Kelchner, Plimpton and Hamilton (1998) and 2 in Miller, Shilkrot and Curtin (2004). In this approach, the magnitude of K is usually determined numerically to achieve both simulation stability and contact compatibility. Eventually, a range of magnitude can be used for K and convergence becomes the decisive issue. Extra numerical experiments have to be performed to narrow the range of K.

In our investigations, we avoid using the above approach by explicitly solving for the contact force on each atom in contact by considering the penetration depth and its velocity. The penetration depth **d** can be first determined from the atom location and velocity, if no contact is assumed. If there is penetration, it must be eliminated during the time increment, Δt, from $\mathbf{d} = \frac{1}{2}\mathbf{a}\Delta t^2$, where **a** is the acceleration. One can determine the contact force $\mathbf{F}_c = m_a \cdot \mathbf{a} = 2m_a \frac{\mathrm{d}}{\Delta t^2}$, where m_a is the mass of the atom. The contact force can then be decomposed into three components in the Cartesian coordinates based on the local outward normal vector of the indenter surface. Friction laws can be added as appropriate, to the force based contact algorithm.

3 Simulation of nanoindentation

3.1 Cylindrical indenter

When a long rigid cylindrical indenter is indented into a workpiece, the middle section can be assumed to be in the plane-strain condition. In this investigation, as shown in Fig. 4, the indentations were performed along the $[\bar{1}\bar{1}2]$ direction on the FCC copper modeled by the embedded atom method (EAM) potential (Daw and Baskes (1984)) and this problem was modeled as a 2D indentation on the (111) plane. The drag coefficient B in Eq. (9) for copper is taken at 1.5×10^{-4} Pa·s (Fusenig and Nembach (1975)). The simulations were conducted at 0 ° K.

Fig. 5 (a) shows a typical load-depth curve from simulation. The initial loading curve is relatively smooth and no dislocations were observed in the atomistic region. The atom distribution corresponding to point A is plotted in Fig. 5 (b). At the first drop, point B in the load-depth curve, dislocation twinning below the indenter was observed, as in Fig. 5 (c). The first dislocation moves along the $[01\bar{1}]$ direction. The other dislocation is nucleated immediately after the first one and it moves along $[1\bar{1}0]$ (negative X) direction. These two dislocations advanced

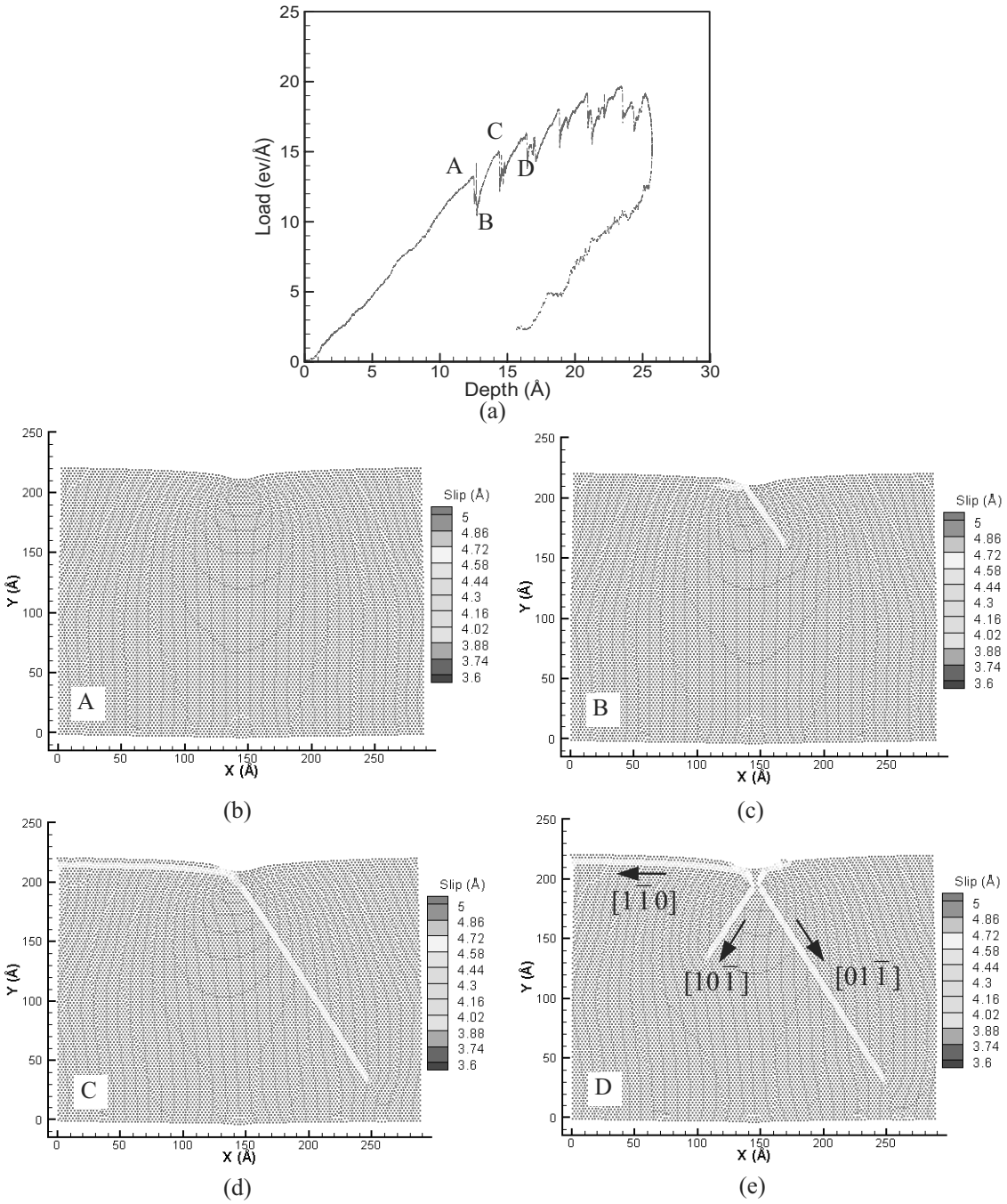

Figure 5 : (a) Load-depth curve using a cylindrical indenter; (b)-(e) Workpiece showing the indent and generation of dislocations at different stage of indentation

in a straight path as the indenter continues to indent into the workpiece. The workpiece stiffens until the next dislocation is generated at points C and D with these states shown in Fig. 5 (d) and (e). The next dislocation is in the $\left[10\overline{1}\right]$ direction, as shown in Fig. 5 (e). All subsequent dislocations are in these three directions and the workpiece softens when each dislocation was generated below the indenter. The initial portion of the unloading in the load-depth curve is related to the velocity of the indenter as it will be discussed later. In the constant unloading portion, the load-depth curve is parallel to the elastic loading part.

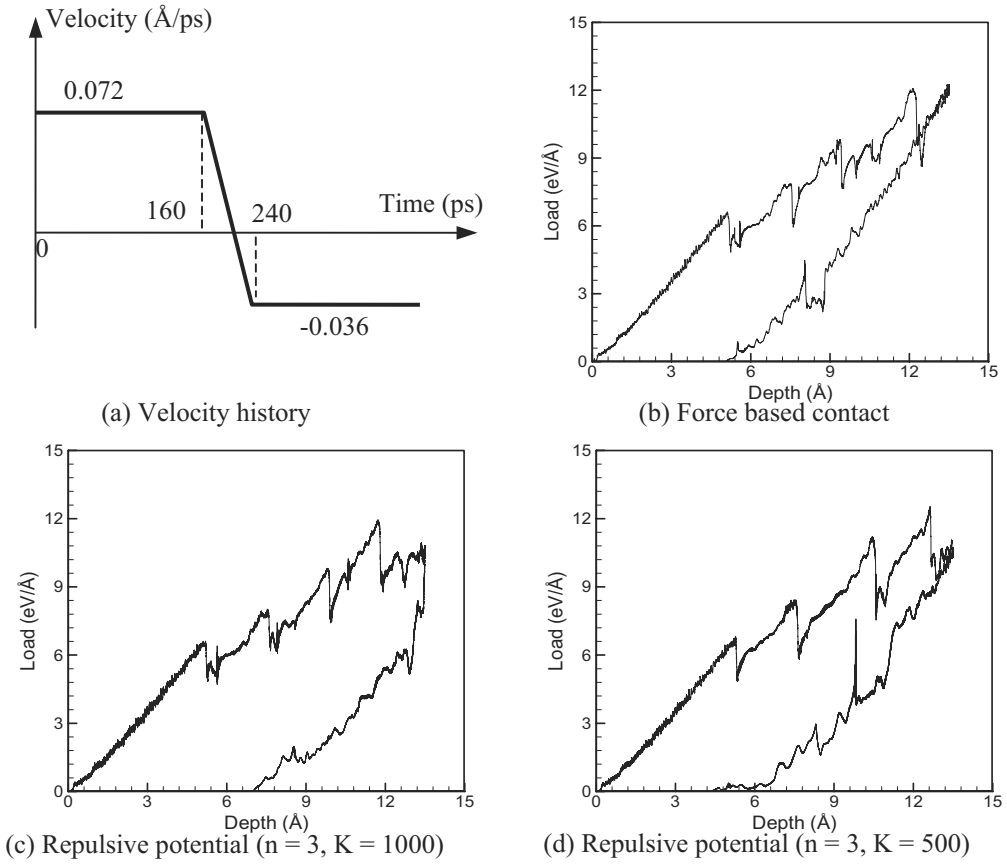

(a) Velocity history (b) Force based contact

(c) Repulsive potential (n = 3, K = 1000) (d) Repulsive potential (n = 3, K = 500)

Figure 6 : Comparison of load-depth curves using different contact algorithms

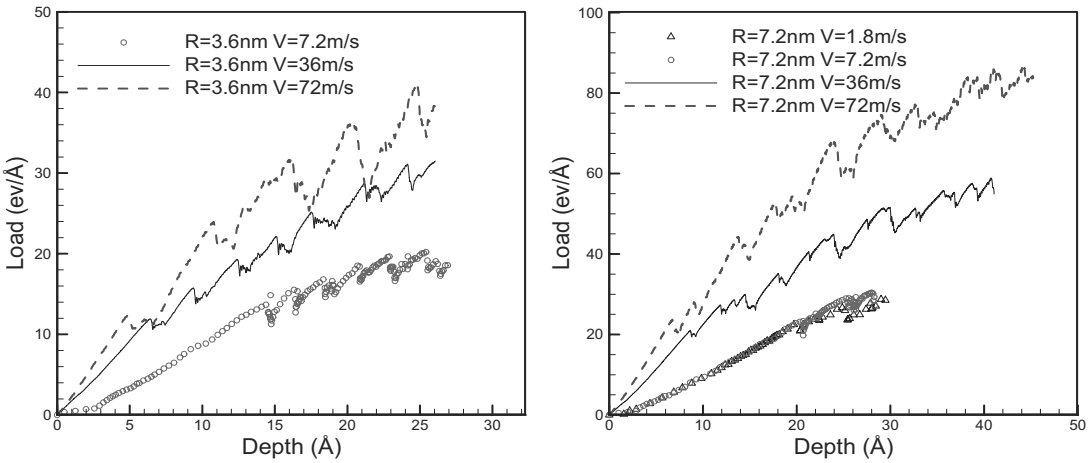

(a) R = 3.6 nm (b) R = 7.2 nm

Figure 7 : Effect of the indentation velocity on the load-depth curve

The next numerical example is to validate the force-based contact algorithm by comparing with the results from the repulsive potential based contact algorithm (Kelchner, Plimpton and Hamilton (1998)). The velocity history of the rigid indenter is shown in Fig. 6 (a). The load-depth curves from three simulations with different contact conditions are shown in Fig. 6 (b), (c), and (d), respectively. All three simulations give similar magnitudes of load and dislocation patterns. When the repulsive contact potential is used, the loading curve appears

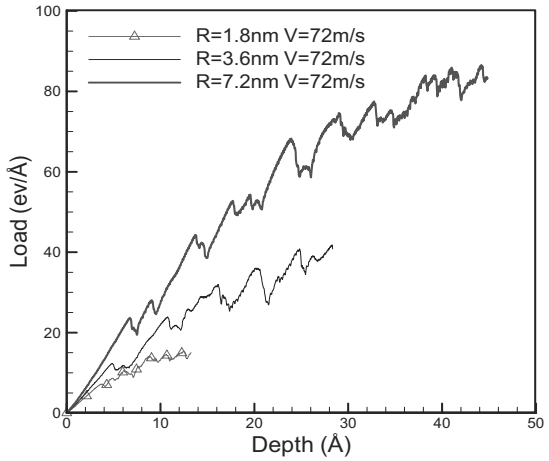

Figure 8 : Effect of the indenter size on the load-depth curve

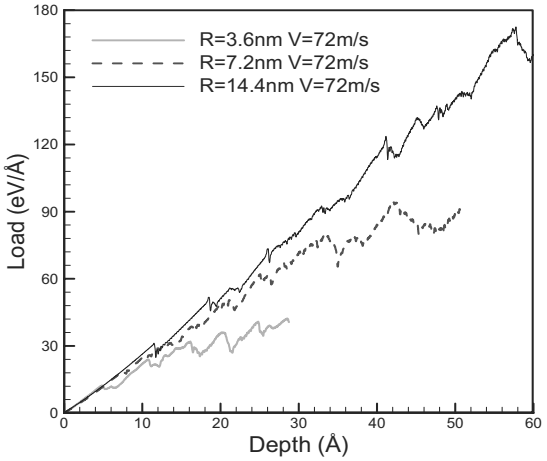

Figure 9 : Load-depth curves when the ratio of the workpiece size and to the indenter radius is a constant

to be smoother for K = 500 than for K = 1000, where K is defined in Eq. (10). The initial portions of the unloading curves are quite different when K is different, as can be seen in Fig. 6 (c) and (d). For this reason, the contact force based algorithm was used in subsequent simulations.

To investigate the effect of indentation velocity, simulations were performed with several indentation velocities with a fixed indenter radius. The overall workpiece size is also fixed at 86.8 nm $\times$ 57.8 nm. The size of the MD region is 28.9 nm $\times$ 21.7 nm. The MD time step is 2 fs (1 fs = 10^{-15} s) and the temporal refinement factor is 5, i.e., the GIMP time step is 10 fs. First, an indenter with a radius of 3.6 nm is used in the simulations at three indentation velocities, 7.2 m/s, 36 m/s and 72 m/s. Fig. 7 (a) shows the indentation load-depth curves at different velocities of indentation. It can be seen that the indentation load is higher if the indentation velocity is higher at a fixed depth of indentation. Another observation is that the indentation depth at the onset of the first slippage in the workpiece is larger, if the indentation speed is lower. Under this condition, the deformation can propagate further so that there is less strain gradient in the workpiece. Same phenomena are observed for these three indentation velocities when the indenter radius is changed to 7.2 nm. However, if the indentation speed is further reduced to 1.8 m/s, the load-depth curve is almost identical to the one with the indentation speed of 7.2 m/s, as shown in Fig. 7 (b). This indicates a quasi-static condition has been reached and the load-depth curve is converged.

Fig. 8 shows three load-depth curves for three different indenter radii when the indentation speed was fixed at 72 m/s. Size of the workpiece is the same as the one used in Fig. 7. In this case, there is a strong dependence on the indenter size. The slope of the load-depth curves in the elastic region increases with indenter radius.

In the theory of elasticity, assuming that the workpiece is an infinite half space, the relation between indentation load P, depth h, and indenter radius R is given as (Gladwell (1980))

$$P = C\left(h - \frac{1}{2}\frac{h^2}{R}\right), \tag{11}$$

where C is a constant depending on the material properties only. It can be seen that when the indentation depth h is much smaller than the indenter radius R, the indentation load P is linearly dependent on h. To investigate the effect of the workpiece boundaries on the simulation, the indenter radius and the workpiece size are changed simultaneously so that their ratio is a constant. Under this condition, each simulation would experience the same amount of boundary effect relatively. Fig. 9 shows the results for three indenter radii, namely, 3.6 nm, 7.2 nm, and 14.4 nm when the indentation velocity is fixed at 72 m/s. It can be seen that the slopes for the three curves are the same before slippage occurs, which is consistent with the predictions in elasticity.

To further verify the coupling model, pure MD simulation was performed with an indenter radius of 7.2 nm. From the load-depth curves in Fig. 10, a reasonably good

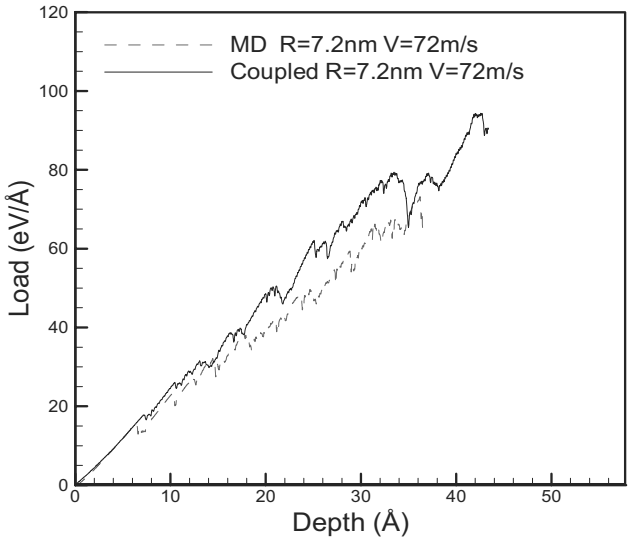

Figure 10 : Comparison of the load-depth curves between the coupled simulations and purely MD simulations

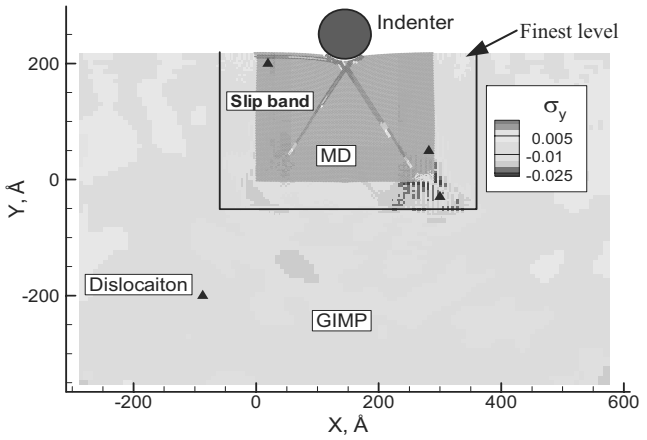

Figure 11 : Slip bands, discrete dislocations and stress distributions in the cylindrical indentation model

agreement between the coupling and the purely MD simulation can be seen.

As discussed in previous sections, the load-depth curves drop slightly when the dislocations are generated below the indenter. Despite different indenter radii and indentation velocities used, the slip patterns are similar in the model. Fig. 11 shows the overall model in the simulation with three slip bands in the MD region. Distributions of the normal stress in the Y-direction, σ_Y in the GIMP region and locations of the discrete dislocations (represented by the solid triangles) are also shown in Fig. 11.

3.2 Wedge indenter

The force based contact algorithm can be applied to wedge indenters by computing the penetration depth **d** based on the outward normal vectors of the wedge surfaces. A wedge indenter with an included tip angle of 120 degrees was used in the simulation. Fig. 12 (b)-(f) shows the slip patterns in the MD region at various indentation depths. Comparing with Fig. 5, slip occurs shortly after the wedge indenter touches the workpiece. The first slippage was initiated at a depth of $\sim$4 Å. More slippage was developed subsequently along the three possible slip directions. Significant amount of slip was developed on the contact surface, resulting in the pile-ups of the material, which is different for the case of cylindrical indenter.

3.3 Finite temperature

In conducting multiscale simulations at finite temperatures, thermal vibrations of atoms can cause adverse effects in coupling because vibrations can generate instantaneous oscillations in the magnitude of strain and stress. Thermostat algorithms have been proposed in the literature (Bernstein, Aziz and Kaxiras (2000); Plimpton (2005)) to control thermal vibrations by removing some kinetic energy in the MD system. For example, the atom velocities can be rescaled to keep the instantaneous temperature at a constant (Bernstein, Aziz and Kaxiras (2000); Plimpton (2005)), or a damping factor can be used to dissipate extra kinetic energy (Jang and Voth (1997); Shiari, Miller and Curtin (2005)). Since the instantaneous temperature is proportional to the kinetic energy, and the MD region is relatively small in coupling, the temperature can increase quickly in the simulation of indentation when the indentation velocity is high. Fig. 13 shows the temperature change during simulation of 2337 Cu atoms using a wedge indenter at three indentation velocities. At the indentation velocity of 360 m/s, large portion of atoms has started to translate at the same simulation time, resulting in higher instantaneous temperatures. Shiari, Miller and Curtin (2005) reported a similar phenomenon with a cylindrical indenter at an indentation speed of 3000 m/s.

The atom velocities are composed of two parts, one representing the thermal vibration and the other representing deformation and translation. Thermostat algorithms do not distinguish between these two. Ideally, the de-

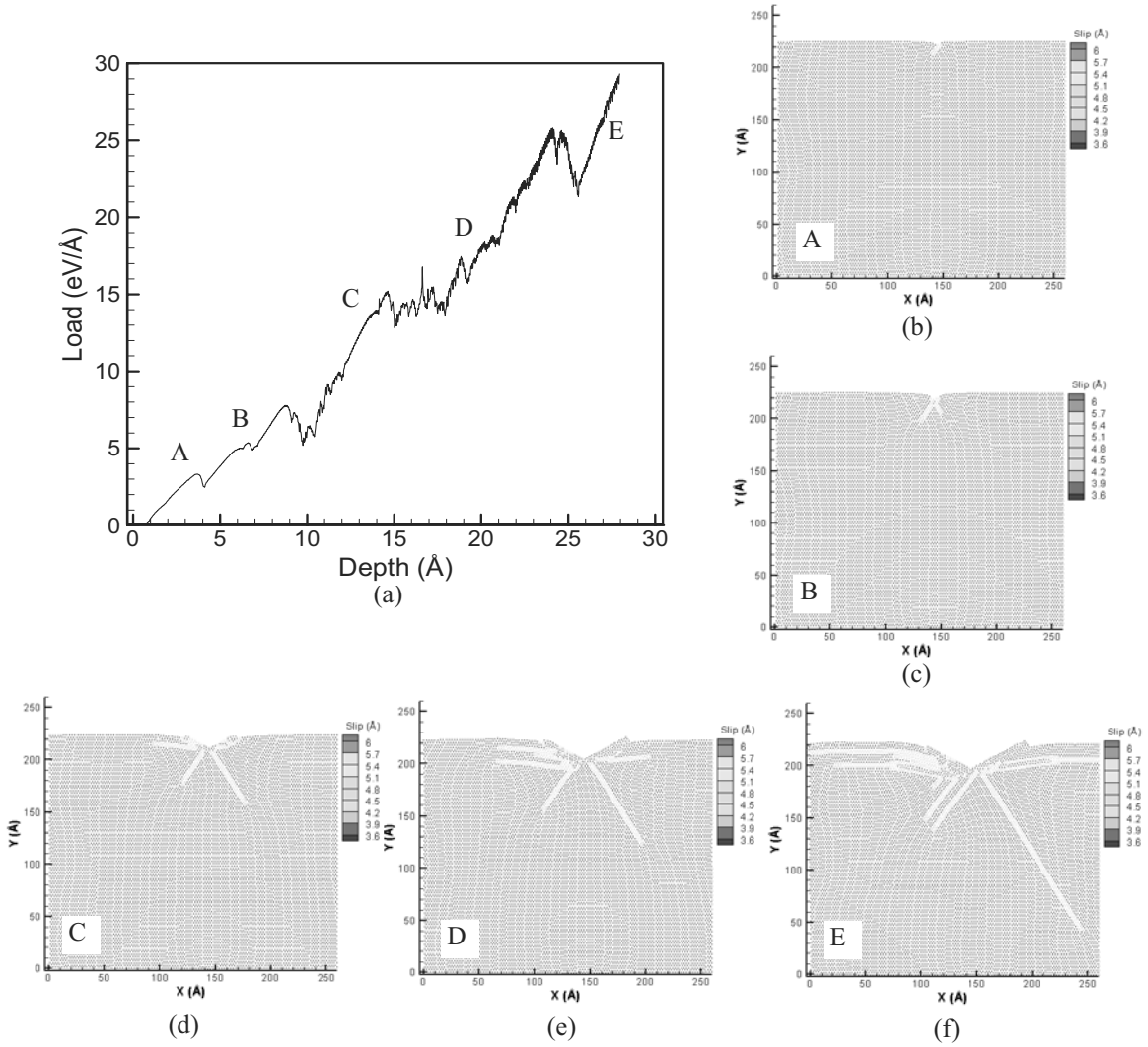

Figure 12 : (a) Load-depth curve using a wedge indenter; (b)-(f) Workpiece showing the indent and generation of dislocations at different stage of indentation

formation part of the velocity should not be altered in the coupling simulation in order to maintain displacement compatibility with the continuum region. Filtering algorithms, such as moving time average and Fourier transform, can be used to separate the thermal vibration from deformation/translational motion in the frequency domain. However, these algorithms require storage of history data for each atom and they are very computationally intensive for coupling simulations.

In this investigation, in order to maintain displacement compatibility between the continuum and atomistic regions, thermostat algorithms are not used. To minimize the effect due to atomic vibrations in the transition region, a spatial average velocity of each atom in the inner zone is used. The average velocity is computed with the first nearest neighboring atoms. For the 2D triangular lattice, each atom has six first nearest neighboring atoms. In addition, the process of interpolating atom velocities to the background grid can reduce the atom vibrations because each background node receives interpolation from multiple atoms. This technique does not allow heat exchange between MD and GIMP and it is only suitable for problems that do not involve much temperature change in nature, such as the indentation problem.

Fig. 14 shows the load-depth curves at different temperatures. The indentation velocity was chosen as 36 m/s because the instantaneous temperature does not vary much at this speed as can be seen in Fig. 13. The

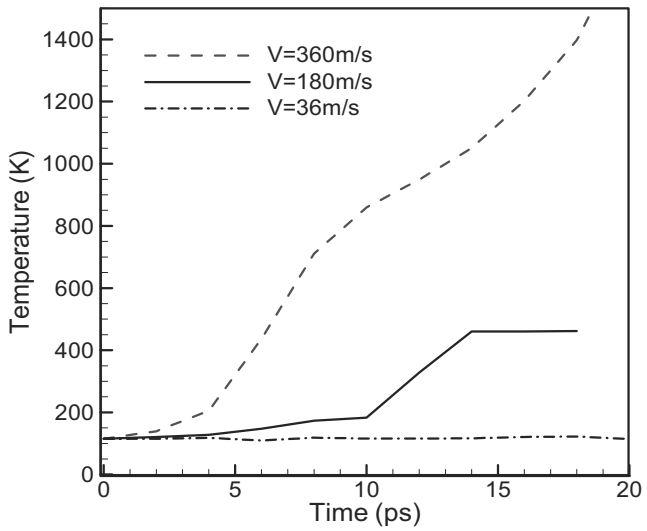

Figure 13 : Instantaneous temperatures as functions of time at different indentation velocities

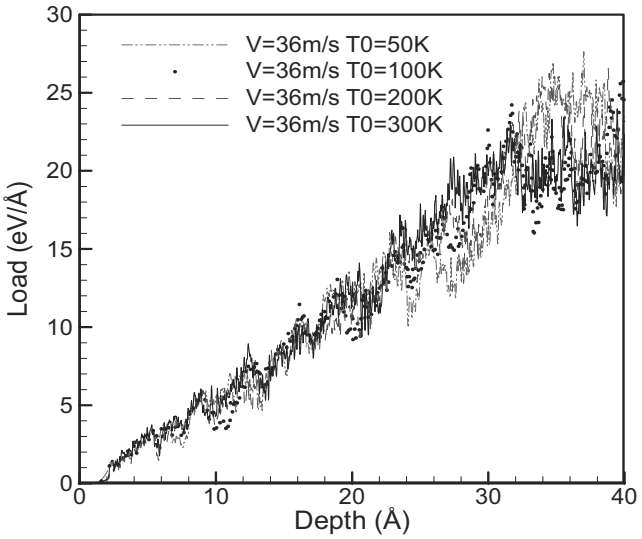

Figure 14 : Load-depth curves at different temperatures using a wedge indenter

load-depth curves at the four initial temperatures overlap each other. The onset of dislocations appears to be independent of temperature when a wedge indenter is used. Shiari, Miller and Curtin (2005) reported strong dependence of the onset of dislocations on the temperature when a cylindrical indenter was used. The coupled simulations in this work show a similar temperature dependence in slip patterns. Fig. 15 shows the slip patterns at a simulation time of 50 ps and an indentation depth of 18 Å at four temperatures. The slip patterns are different at different temperatures even when the applied indentation load is nearly identical.

4 Conclusions

A multiscale simulation algorithm coupling molecular dynamics (MD) at the atomistic scale, discrete dislocation (DD) at the meso scale and generalized interpolation material point (GIMP) method at the macro scale is developed for material simulations based on prior coupling method between MD and GIMP (Ma, Lu, Wang, Hornung, Wissink and Komanduri (2006)). Force and displacement compatibilities are ensured at the transition region. 2D indentation problems were investigated using the multiscale simulation algorithm using a cylindrical indenter and a wedge indenter.

1. Discrete dislocations are coupled with GIMP based on the principle of superposition proposed by van der Giessen and Needleman (1995). The total displacement and traction generated by the dislocations and GIMP on the boundary equal to the externally applied displacement and traction, respectively. Discrete dislocations are coupled with MD using the detection algorithm proposed by Shilkrot, Miller and Curtin (2004).

2. A coupling algorithm incorporating GIMP, DD, and MD is developed with parallel processing using a common domain decomposition scheme. In parallel processing, each processor updates all the material points, discrete dislocations, and atoms in its subdomain.

3. The coupling algorithm is used to simulate the indentation on Cu (111) plane with a cylindrical indenter and a wedge indenter. Initially, dislocation nucleation and subsequent propagation of dislocations are observed for the indentation simulation using both indenters.

4. For simulations with a cylindrical indenter, the effects of indenter radius, indentation speed, and temperature on the dislocation patterns and the load-depth curve are investigated. The effect of the size of the workpiece on the load-depth curve was also studied. Dislocation twinning that occurs below the indenter can be related to the drops in the load-depth

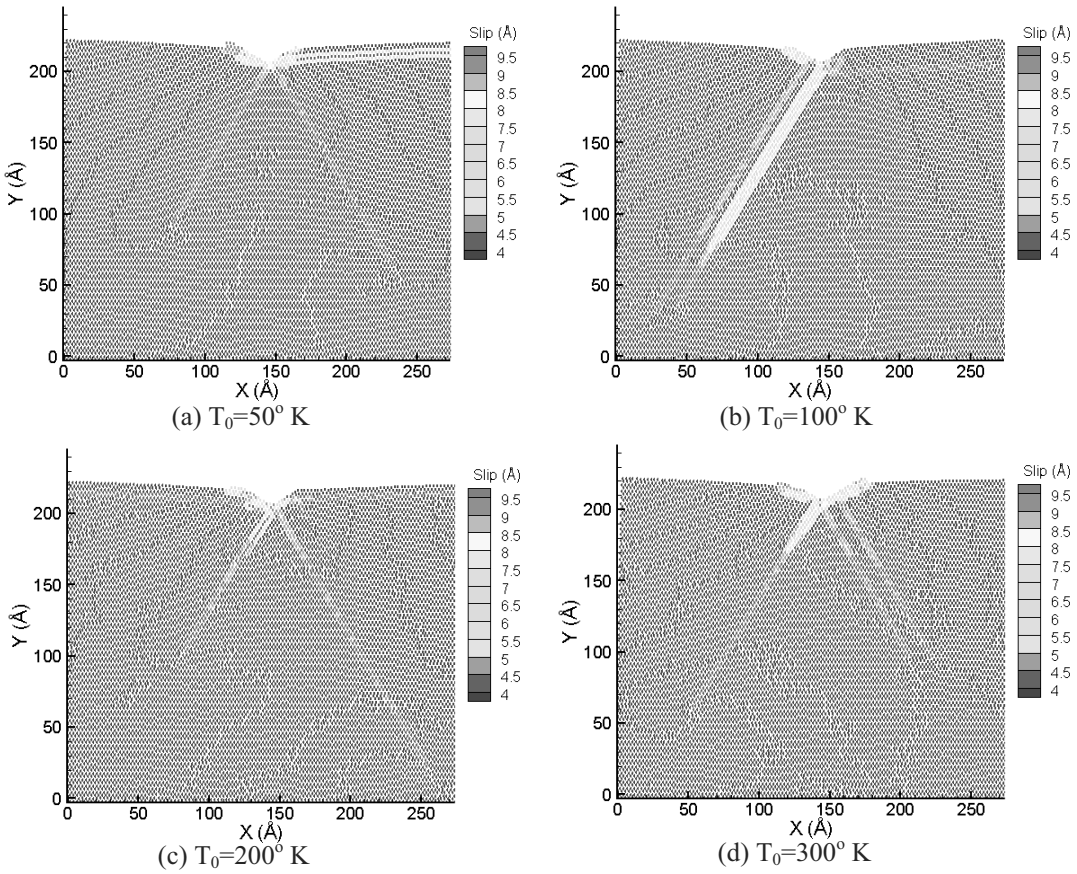

(a) T_0=50^o K (b) T_0=100^o K

(c) T_0=200^o K (d) T_0=300^o K

Figure 15 : Slip patterns at different temperatures when the indentation depth is 18 Å

curve, i.e., the generation of a new dislocation below the indenter causes an instant drop in the load-depth curve. Slip bands in three directions are developed in the MD region due to indentation and they are independent of indenter radius and velocities.

5. Spatial averaging technique is used to maintain displacement compatibility at finite temperatures. In the transition region, the atom velocity is averaged with six nearest neighboring atoms in 2D for coupling to reduce the adverse effect of thermal vibrations on the continuum region. This technique is appropriate for simulations of problems under isothermal conditions, such as nanoindentation.

Acknowledgement: The work was supported by a grant from the Air Force Office of Scientific Research (AFOSR) through a DEPSCoR grant (No. F49620-03-1-0281). The authors would like to thank Dr. Craig S. Hartley, Dr. Jamie Tiley Jr., and Dr. Brett Conner, Program Managers (during the course of the project) for the Metallic Materials Program at AFOSR for the support of and interest in this work. R.K. acknowledges the A.H. Nelson, Jr., Endowed Chair in Engineering for additional support. The authors also acknowledge Dr. Richard Hornung and Dr. Andy Wissink of the Lawrence Livermore National Laboratory for providing the SAMRAI code, and Dr. Steve Plimpton of the Sandia National Laboratory for providing the LAMMPS MD simulation code.

References

Amodeo, R.J.; Ghoniem, N.M. (1990): Dislocation dynamics. I. A proposed methodology for deformation micromechanics. *Physical Review B*, v41, pp.6958-6966.

Bardenhagen, S.G.; Kober, E.M. (2004): The generalized interpolation material point method. *CMES: Computer Modeling in Engineering & Sciences,* v5, n6, pp.477-496.

Bernstein, N.; Aziz, M.J.; Kaxiras, E. (2000): Atomistic simulations of solid-phase epitaxial growth in silicon. *Physical Review B*, v61, n10, pp.6696-6700.

Cai, W.; de Koning, M.; Bulatov, V.V.; Yip, S. (2000): Minimizing boundary reflections in coupled-domain simulations. *Physical Review Letters*, v85, n15, pp.3213-3216.

Curtin, W.A.; Miller, R.E. (2003): Atomistic/continuum coupling in computational materials science. *Modeling and Simulation in Materials Science and Engineering*, v11, R33-R68.

Daw, M.S.; Baskes, M.I. (1984): Embedded-atom method: derivation and application to impurities, surfaces, and other defects in metals. *Physical Review B*, v29, pp.6443-6453.

Fang, X.F.; Dahl, W. (1993): Investigation of the formation of dislocation cell structures and the strain hardening of metals by computer simulation. *Materials Science and Engineering A*, v164, pp.300-305.

Fusenig, K.D.; Nembach, E. (1975): Dynamic dislocation effects in precipitation hardened materials, *Acta Metallurgica et Materialia*, v41, pp.3181-3189.

Gladwell, G.M.L. (1980): *Contact Problems in the Classical Theory of Elasticity*, Sijthoff & Noordhoff.

Groma, I.; Pawley, G.S. (1993): Role of the secondary slip system in a computer simulation model of the plastic behaviour of single crystals. *Materials Science and Engineering A*, v164, pp.306-311.

Gulluoglu, A.N.; Hartley, C.S. (1992): Simulation of dislocation microstructures in two dimensions. I. Relaxed structures. *Modelling and Simulation in Materials Science and Engineering*, v1, n1, pp. 1-17.

Gulluoglu, A.N.; Hartley, C.S. (1993): Simulation of dislocation microstructures in two dimensions: II. Dynamic and relaxed structures. *Modeling and Simulation in Materials Science and Engineering*, v1, pp.383-402.

Hasebe, T. (2006): Multiscale crystal plasticity modeling based on field theory. *CMES: Computer Modeling in Engineering and Sciences*, v11, n3, pp.145-155.

Hirth, J.P.; Lothe, J. (1982): *Theory of Dislocations*. John Wiley & Sons, 2^{nd} ed.

Jang, S.; Voth, G.A. (1997): Simple reversible molecular dynamics algorithms for Nosé-Hoover chain dynamics, *Journal of Chemical Physics*, v107, n22, pp.9514-9526.

Kelchner, C.; Plimpton, S.; Hamilton, J. (1998): Dislocation nucleation and defect structure during surface indentation**,** *Physical Review B*, v58, n17, pp.11085-11088.

Kohlhoff, S.; Gumbsch, P.; Fischmeister, H.F. (1991): Crack propagation in b.c.c. crystals studied with a combined finite-element and atomistic model. *Philosophical Magazine A: Physics of Condensed Matter, Defects and Mechanical Properties*, v64, n4, pp.851-878.

Kubin, L.P.; Canova, G. (1992): The modelling of dislocation patterns. *Scripta metallurgica,* v27, pp.957-962.

Liu, Y.; Wang, B.; Yoshino, M.; Roy, S.; Lu, H.; Komanduri, R. (2005): Combined numerical simulation and nanoindentation for determining mechanical properties of single crystal copper at mesoscale. *Journal of the Mechanics and Physics of Solids*, v53, n12, pp.2718-2741.

Lu, H.; Daphalapurkar, N.P.; Wang, B.; Roy, S.; Komanduri, R. (2006): Multiscale simulation from atomistic to continuum - Coupling molecular dynamics (MD) with the material point method (MPM). *Philosophical Magazine*, v86, n20, pp. 2971-2994.

Ma, J.; Lu, H.; Komanduri, R. (2006): Structured mesh refinement in generalized interpolation material point (GIMP) method for simulation of dynamic problems. *CMES: Computer Modeling in Engineering & Sciences*, v12, n3, pp. 213-227.

Ma, J.; Lu, H.; Wang, B.; Hornung, R.; Wissink, A.; Komanduri, R. (2006): Multiscale simulation using generalized interpolation material point (GIMP) method and molecular dynamics (MD). *CMES: Computer Modeling in Engineering & Sciences*, in press.

Ma, J.; Lu, H.; Roy, S.; Hornung, R.; Wissink, A.; Komanduri, R. (2005): Multiscale simulations using generalized interpolation material point (GIMP) method and SAMRAI parallel processing. *CMES: Computer Modeling in Engineering & Sciences,* v8, n2, pp.135-152.

Miller, R.E.; Shilkrot, L.E.; Curtin, W.A. (2004): A coupled atomistics and discrete dislocation plasticity simulation of nanoindentation into single crystal thin films. *Acta Materialia*, v52, n2, pp.271-284.

Plimpton, S.J. (1995): Fast Parallel Algorithms for Short-Range Molecular Dynamics. *Journal of Computational Physics*, v117 n1, pp. 1-19.

Plimpton, S.J. (2005): Documentation for the LAMMPS Molecular Dynamics Simulator, Sandia National Laboratory.

Rafii-Tabar, H.; Hua, L.; Cross, L. (1998): A multi-scale atomistic-continuum modeling of crack propagation in a two-dimensional macroscopic plate. *Journal of Physics: Condensed Matter*, v10, pp.2375-2387.

Raff, L.M.; Malshe, M.; Hagan, M.; Doughan, D.I.; Rockley, M.G.; Komanduri, R. (2005): Ab initio potential-energy surfaces for complex, multichannel systems using modified novelty sampling and feedforward neural networks. *Journal of Chemical Physics*, v122, n8, pp.084104.

Shen, S.; Atluri, S.N. (2004a): Computational nano-mechanics and multi-scale simulation. *CMC: Computers, Materials, & Continua*, v1, n.1, pp.59-90.

Shen, S.; Atluri, S.N. (2004b): Atomic-level stress calculation and continuum-molecular system equivalence. *CMES: Computer Modeling in Engineering & Sciences*, v6, n1, pp.91-104.

Shen, S.; Atluri, S.N. (2004c): Multiscale simulation based on the meshless local petrov-galerkin (MLPG) method. *CMES: Computer Modeling in Engineering and Sciences*, v5, n3, pp.235-255.

Shen, S.; Atluri, S.N. (2005): A tangent stiffness MLPG method for atom/continuum multiscale simulation. *CMES: Computer Modeling in Engineering & Sciences*, v7, n1, pp.49-67.

Shiari, B.; Miller, R.E.; Curtin, W.A. (2005): Coupled atomistic/discrete dislocation simulations of nanoindentation at finite temperature, *Journal of Engineering Materials and Technology, Transactions of the ASME*, v127, n4, pp.358-368.

Shilkrot, L.E.; Miller, R.E.; Curtin, W.A. (2004): Multi-scale plasticity modeling: coupled atomistics and discrete dislocation mechanics. *Journal of the Mechanics and Physics of Solids*, v52, pp.755-787.

Sulsky, D.; Schreyer, H.L. (1996): Axisymmetric foam of the material point method with applications to upsetting and Taylor impact problems. *Computer Methods in Applied Mechanics and Engineering,* v139, pp. 409-429.

Sulsky, D.; Zhou, S.J.; Schreyer, H.L. (1995): Application of a particle-in-cell method to solid mechanics. *Computer Physics Communications,* v87, pp.236-252.

Tewary, V.K.; Read D.T. (2004): Integrated Green's function molecular dynamics method for multiscale modeling of nanostructures: application to Au nanoisland in Cu. *CMES: Computer Modeling in Engineering & Sciences*, v6, n4, pp.359-371.

van der Giessen, E.; Needleman, A. (1995): Discrete dislocation plasticity: a simple planar model. *Modeling and Simulation in Materials Science and Engineering*, v3, pp.689-735.

Zbib, H.M.; Diaz de la Rubia, T. (2002): A multiscale model of plasticity. *International Journal of Plasticity*, v18, n9, pp.1133-1163.

Zbib, H.M.; Rhee, M.; Hirth, J.P. (1998): On plastic deformation and the dynamics of 3D dislocations. *International Journal of Mechanical Sciences,* v40, pp.113-127.